Discrete RF Coil Components Introduce Significant Noise and Artifacts into PET Images in Combined PET-MRI Systems

Geron A. Bindseil[1], William B. Handler[1], and Blaine A. Chronik[1,2]

[1]*Department of Physics and Astronomy, University of Western Ontario, London, Ontario, Canada,* [2]*Robarts Research Institute, University of Western Ontario, London, Ontario, Canada*

Introduction

Combining MRI and positron emission tomography (PET) is an active area of research and development. In simultaneous PET-MRI, the RF coil must be located inside the PET detector ring. While this can be avoided in sequential PET-MRI with two separate scanners, it is sometimes desirable to have an RF coil built into the patient or animal handling system which remains in place during PET acquisition. Herrick, *et al.* have used a Monte Carlo simulation to show that the presence of RF coil materials within a PET detection system can result in a significant increase in photon scattering [1]. Increased scattering and absorption result in greater image noise and lower detection sensitivity. Furthermore, many RF coils consist of a symmetrical arrangement of discrete highly attenuating components: copper, solder and capacitors. MRI-based attenuation correction schemes are further complicated by the fact that the RF coil does not appear in the MR image. The authors have developed a comprehensive Monte Carlo simulation workflow utilizing the histogramming and image reconstruction software of the commercial system modeled to investigate and identify any significant effects the RF coil components have on PET image quality.

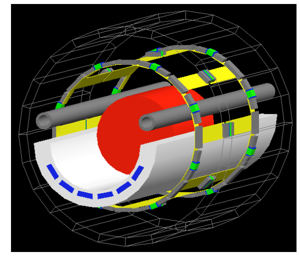

Fig 1. Simulation geometry.

Methods

Monte Carlo Simulation Architecture

Simulated PET data were generated with the GEANT4 Application for Tomographic Emission (GATE) package, which is based on the GEANT4 Monte Carlo toolkit [2]. There are three stages to PET image generation: data acquisition, histogramming data into sinograms and reconstruction. The Siemens Inveon dedicated small-animal PET scanner was modeled. In order to make the image generation workflow as close as possible to an experimental PET workflow, simulated emission data were first converted to the raw list-mode data format of the commercial PET scanner and then all histogramming and reconstruction were performed in the commercial software. Normalization of the PET detection scheme was accomplished by acquiring simulated coincidence data from a uniform cylindrical distribution of activity (radius: 3 cm, length: 12.7 cm) for a total of 2.3 billion coincidences, followed by conversion to list-mode format and histogramming by cylinder inversion in the commercial software. Attenuation correction sinograms were generated within GATE by a custom algorithm that computes the attenuation correction factor for each line of response (crystal center to crystal center) using the material definitions, phantom geometry and interaction cross-sections used internally by the emission simulation. Reconstruction was performed in the commercial software using the two-dimensional Ordered Subset Expectation Maximization (OSEM2D) method with default settings (16 subsets and 4 iterations).

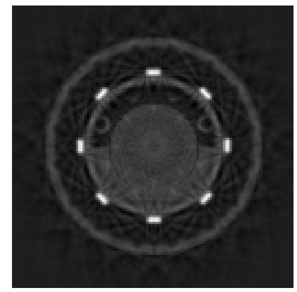

Fig 2. Attenuation map of RF coil, bed and phantom (filtered backprojection reconstruction).

PET System Model

The PET detector has a 16-cm-diameter bore, a 12.7-cm axial field of view and is composed of 4 axial 16-block rings with each block containing a 20 x 20 array of lutetium oxyorthosilicate (LSO) scintillator with dimensions (1.51 x 1.51 x 10) mm. The radioactivity in LSO was not simulated. The coincidence timing and energy windows were 3.43 ns and 350-650 keV with a 14.6% energy blurring.

Phantom and RF Coil Model

The mouse-sized phantom, shown in blue in Figure (1), consisted of a water-filled acrylic cylinder (inner radius: 15 mm, outer radius: 16.75 mm, length: 60 mm) centered in the field of view. The water volume contained a uniform initial activity of the positron emitter F-18 at 3.7 MBq with each simulation lasting 20 minutes. The decay of F-18 and positron annihilation were simulated. The phantom was located on slightly larger animal bed consisting of a 6.35-mm-thick acrylic half-tube with six small lengthwise internal channels for heating water. The bed also contained two delrin tubes for anaesthetic gas. An RF coil was modeled as an 8-rung birdcage coil just wide enough to contain the bed and phantom. The conductor consisted of copper tape (thickness: 0.2 mm, width: 6 mm), shown yellow, placed on a 3-mm-thick acrylic former, not shown. Two 5-mm-thick end plates, not shown, supported a RF shield (copper thickness: 0.03 mm) at 1.4 times the radius of the RF coil supported by a 3-mm-thick acrylic former, shown in wireframe. Sets of two capacitors (combined dimensions: 1.86 x 2.55 x 5.1 mm) were placed at the center of each rung and between each rung connection on each end ring of the coil. The capacitor material was chosen to be a 50/50 mixture of $BaTiO_3$ and $Pd_{70}Ag_{30}$ for the body, shown green, and $Cu_{90}Sn_{10}$ for the terminators, shown blue. Lead-free $Sn_{95.8}Ag_{3.5}Cu_{0.7}$ solder joints (thickness: 1.5 mm), shown grey, connected each conductor rung to the end rings and each capacitor to the copper conductor.

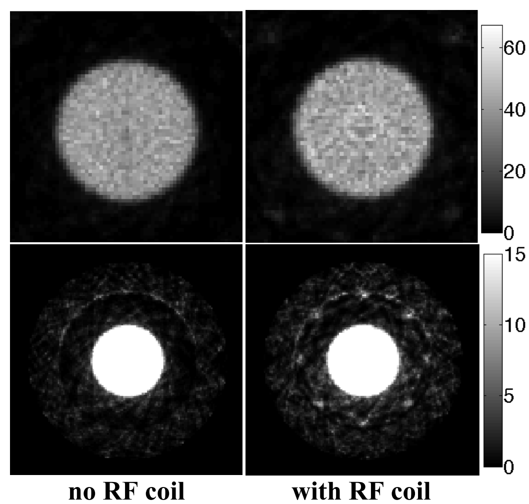

Fig 3. Reconstructed PET images showing the central axial slice. The greyscale has units Bq/voxel. The images on the left correspond to the simulation with no RF coil present, and those on the right are for the case with the RF coil. The top row shows the PET images with a zoom factor of 2 and full greyscale. Increased noise (25% higher standard deviation) and a crescent-shape artifact are apparent in the RF coil image (top right) when compared to the case with no RF coil (top left). The bottom row shows the full field of view windowed to make the background noise visible. The case with the RF coil (bottom right) shows significantly increased noise outside the phantom when compared with the case with no RF coil (bottom left). A symmetric artifact arising from the ring of 8 capacitors is evident.

Image Analysis

Two cases were modeled: with the RF coil and without the RF coil. Statistics were recorded for prompts (total coincidences), scatters (coincidences with at least one Compton scatter interaction), randoms (coincidences originating from different decays) and trues (valid coincidences with no scattering). Each image was scaled so that the total activity in the region of activity matched the known activity. The standard deviation of the reconstructed activity in the voxels in the region of activity was computed.

Results

The simulation with no RF coil had had 207×10^6 prompts, 168×10^6 trues, 36×10^6 scatters and 4.2×10^6 randoms. The simulation with the RF coil present had 190×10^6 prompts, 140×10^6 trues, 47×10^6 scatters and 3.9×10^6 randoms. The scatter fraction was approximately 40% greater for the simulation with the RF coil. Figure 3 shows the reconstructed PET images for both cases. The standard deviations of the activity in the case with no RF coil and with the RF coil were 4.0 Bq/voxel and 5.0 Bq/voxel, respectively, where the actual activity in each voxel of water was 41.9 Bq.

Conclusions

A Monte Carlo simulation that used the histogramming and reconstruction software of the commercial system modeled showed that the presence of discrete RF coil components, specifically capacitors and solder, within the PET detector results in a significant increase in image noise and a potential for image artifacts. This study suggests that birdcage RF coils with capacitors located in the middle of the rungs are not suitable for combined PET-MRI. Care must also be taken when designing array coils for PET-MRI due to the high number of discrete capacitor components surrounding the subject in close proximity.

References

[1] Herrick, P. *et al.* 2011 Proc. 19th ISMRM, 3801.
[2] Jan, S. *et al* 2004 *Phys. Med. Biol.* **49** 4543.

Acknowledgements

The authors gratefully acknowledge funding from NSERC Canada.